Unilateral Exposure of *Shaker* B Potassium Channels to Hyperosmolar Solutions

John G. Starkus,* Thomas Schlief,‡ Martin D. Rayner,*§ and Stefan H. Heinemann‡
*Békésy Laboratory of Neurobiology, Pacific Biomedical Research Center and §Department of Physiology, School of Medicine, University of Hawaii, Honolulu, Hawaii 96822-2359; and ‡Max-Planck-Gesellschaft, Arbeitsgruppe Molekulare und Zelluläre Biophysik, Drackendorfer Strasse 1, D-07747 Jena, Germany

ABSTRACT This study tests the hypothesis that ion channels will be affected differently by external (extracellular) versus internal (cytoplasmic) exposure to hyperosmolar media. We looked first for effects on inactivation kinetics in wild-type *Shaker* B potassium channels. Although external hyperosmolar exposure did not alter the inactivation rate, internal exposure slowed both onset and recovery from fast inactivation. Differential effects on activation kinetics were then characterized by using a noninactivating *Shaker* B mutant. External hyperosmolar exposure slowed the late rising phase of macroscopic current without affecting the initial delay or early rising phase kinetics. By contrast, internal exposure slowed the initial steps in channel activation with only minimal changes in the later part of the rising phase. Neither external nor internal hyperosmolar exposure affected tail current rates in these noninactivating channels. Additionally, suppression of peak macroscopic current was approximately twofold smaller during external, as compared with internal, hyperosmolar exposure. Single-channel currents, observed under identical experimental conditions, showed a differential suppression equivalent to that seen in macroscopic currents. Apparently, during unilateral hyperosmolar exposure, changes in macroscopic peak current arise primarily from changes in single-channel conductance rather than from changes in equilibrium channel gating. We conclude that unilateral hyperosmolar exposure can provide information concerning the potential structural localization of functional components within ion-channel molecules.

INTRODUCTION

As biological membranes and macromolecular surfaces approach more closely than ~3 nm, their interactions become increasingly dominated by solvent perturbation forces (Parsegian et al., 1986), and when the activity of the solvent is reduced by addition of osmoticants, macromolecules in equilibrating thermodynamic phases must compete for the available solvent molecules. Similarly, functionally significant conformational changes in biological macromolecules may generate competition for stabilizing water molecules if differences in hydration exist between the *"Tense"* and *"Relaxed"* conformational states. Both the cytochrome *c* oxidase reaction (Kornblatt and Hoa, 1990) and the oxygenation of hemoglobin molecules (Colombo et al., 1992) are sensitive to solution osmolarity, suggesting that stabilization of the activated state requires ~10 or 60 water molecules, respectively.

Hyperosmolar stress was first used by Zimmerberg and Parsegian (1986) to investigate the gating behavior of a voltage-sensitive ion channel. In that study, voltage-dependent anion channels were extracted from mitochondrial membranes and reconstituted into artificial bilayers. The voltage-dependent gating behavior of single channels was evaluated after changes in osmotic pressure applied symmetrically to both sides of the bilayer membrane (using solutions of constant ionic strength). Gating of voltage-dependent anion channels was affected by both applied voltage and osmotic stress, suggesting that transitions from the "closed" to the "open" state of the voltage-dependent anion channel involved extraction of a constant water volume from the bulk hyperosmolar medium so as to hydrate and thus stabilize the open state of the channel.

Zimmerberg et al. (1990) next examined the effects of osmotic stress in native delayed-rectifier potassium channels by applying symmetrical hyperosmolar solutions to both the inside and the outside of perfused squid giant axons. This preparation provided large noninactivating macroscopic currents but was not appropriate for single-channel studies. Zimmerberg et al. (1990) demonstrated suppressions of peak potassium current, which were proportional to the applied osmotic stress regardless of the osmoticant used. Although activation seemed slowed by osmotic stress, suppression of macroscopic current did not involve changes in the voltage sensitivity of activation and was not correlated with changes in solution conductivity. They concluded that suppression of peak macroscopic current resulted from changes in the equilibrium opening probability in delayed-rectifier channels, implying an increase in channel hydration (of 40–50 water molecules) associated with the entry into the open state.

In a subsequent study of osmotic effects on native sodium channels in crayfish giant axons, Rayner et al. (1992) removed fast inactivation pharmacologically to permit analysis of equilibrium channel opening. Because of experimental constraints, their data were obtained

Received for publication 6 January 1995 and in final form 2 June 1995.
Address reprint requests to Dr. John G. Starkus, Bekesy Laboratory of Neurobiology, University of Hawaii, 1993 East-West Road, Honolulu, Hawaii 96822-2321. Tel.: 808-956-6398; Fax: 808-956-6984; E-mail: john@ahi.pbrc.hawaii.edu.

0006-3495/95/09/860/13 $2.00

using only internally applied hyperosmolar solutions; however, both sucrose and formamide produced similar suppressions of peak sodium current. Furthermore, internal hyperosmolar exposure slowed sodium channel opening without altering either the voltage-sensitivity of activation or the kinetics of deactivation as seen in tail currents. A simple activation/deactivation model, which assumed electrostatically coupled voltage-sensitive and solvent-sensitive steps, provided a preliminary description of both their kinetic and their equilibrium data. Assuming that suppression of the peak currents resulted from changes in equilibrium between activation and deactivation, this model suggested that between 20 and 30 water molecules would be required to stabilize the open state of the sodium channel.

The present study was initiated to provide a more detailed evaluation of the kinetic effects of hyperosmolar exposure, with use of cloned *Shaker* channels expressed in *Xenopus laevis* oocytes, where both macroscopic and single-channel data could be obtained under identical experimental conditions. We found kinetic changes similar to those described in previous studies, but noted additional, differential effects of unilateral hyperosmolar exposure. These differential responses provide new evidence for the structural localization of functional components within the channel activation mechanism.

Preliminary results of this work have been reported in abstract form (see Starkus et al., 1994, 1995).

METHODS

Molecular biology

The data presented here were recorded from the 29–4 *Shaker* B wild-type channel (Iverson and Rudy, 1990), with its normal inactivation mechanism intact and a noninactivating mutant obtained by deletion of residues 2 through 30 from the amino terminal region of the same 29–4 channel (Schoppa et al., 1992). Additional experiments carried out using the construct *Shaker* BD6–46 (Hoshi et al., 1990) gave similar results.

Methods for preparation of oocytes (from *X. laevis*) and for messenger RNA injection have been described previously (Methfessel et al., 1986; Stühmer et al., 1987).

Electrophysiology

Conventional patch-clamp techniques were used for electrophysiological measurements (Hamill et al., 1981). Macroscopic currents were measured using both inside-out and outside-out configurations. Patch pipettes were fabricated from aluminum-silicate glass with tip diameters between 1 and 3 μm. In standard salines these pipettes had electrical resistances in the range of 2.5–0.8 MΩ. Membrane patches obtained using electrodes of higher resistance lasted longer and were more resilient to bath changes and to hyperosmolar media. Patches with seal resistances smaller than 5 GΩ were discarded.

In this study, hyperosmolar conditions were always applied by changing the bath solution. Thus membrane patches to be exposed to external hyperosmolar solutions were always pulled in the outside-out configuration, whereas the inside-out configuration was used for internal application of hyperosmolar solutions. Two practical considerations favored this decision: first, rapid return to control osmolarity was required to distinguish effects of osmotic exposure from kinetic drifts or channel rundown; and second, addition of hyperosmolar solutions to the pipette could generate standing osmotic gradients along the pipette, resulting from dilution of the osmoticant by entry of bulk water from across the membrane into the small volume of the pipette tip.

All patch experiments were performed at room temperature (20–22°C). Currents from macropatches were recorded with an EPC-9 patch-clamp amplifier (HEKA Elektronik, Lambrecht, Germany). Software for data collection and analysis included Pulse+PulseFit (HEKA Elektronik) and Igor (WaveMetrics Inc., Lake Oswego, OR), both running on either a Macintosh Quadra 700 or Macintosh IIfx computer (Apple Computer Inc., Cupertino, CA). Exponential fits to data traces were made using Templegraph software (Mihalisin Assoc. Inc., Ambler, PA) running on a Sun SPARCstation (Sun Microsystems Inc., Sunnyvale, Ca.). Computer modeling of channel kinetics was carried out on the same computer, using methods previously described by Rayner et al. (1992). All simulations shown here used clamp rise characteristics appropriate to match our patch recordings in which transmembrane voltage settled to within 1% of command potential in ~100 ms.

Single-channel currents were recorded using an EPC-7 patch-clamp amplifier (List, Darmstadt, Germany) with pipettes made of thick-walled borosilicate glass.

Hyperosmolar solutions and "osmotic stress"

Osmotic stress has been defined by Zimmerberg et al. (1990) as the tension that develops within any space from which a given solute is excluded when that space is in equilibrium with a bulk solution having an osmotic pressure resulting from the given solute species. Thus when a defined bathing medium is made hyperosmolar by addition of a nonionic osmoticant, the applied osmotic stress is reported as the difference between the osmolarities of the control and test solutions. However, when ion channels are only unilaterally exposed to hyperosmolar solutions, osmotic gradients will be established across the channels. In this case, osmotically induced water movements may produce local dilutions of the hyperosmolar medium in the microenvironments within and surrounding the channel molecules (producing complex graded interfaces between internal and external solutions of differing osmotic pressure). Under these experimental conditions, applied osmotic stress cannot be well defined. We therefore indicate the total osmolarity of each applied solution.

Control solutions with an osmolarity of ~250 mOsm/kg used in this study are summarized in Table 1. Sucrose was selected as the nonionic osmoticant. Previous studies of osmotic effects on ion channels (Anderson, 1983; Zimmerberg et al., 1990; Rayner et al., 1992), in which sucrose has been compared with other osmoticants, have provided no evidence that might suggest it has additional pharmacological actions. In the figure legends, extracellular and intracellular solutions are separated by a double-slash, e.g., NFR//K-EGTA. All solutions were made hyperosmolar by the addition of dry, reagent-grade sucrose (Sigma, St. Louis, MO). Solution osmolarities were measured using a freezing-point osmometer (mOsmette, Precision Instruments, Sudbury, MA). Because solutions containing a high concentration of sucrose are rather viscous, careful washout procedures are necessary to obtain appropriate posthyperosmolar control data. At least 20 × the bath volume was used in flushing the experimental chamber, and

TABLE 1 Solutions

Solution	NaCl (mM)	KCl (mM)	NMGCl (mM)	$CaCl_2$ (mM)	EGTA (mM)	Hepes (mM)
NFR	115	2.5	0	1.8	0	10
K-Ringer	0	115	0	1.8	0	10
K-EGTA	0	115	0	0	1.8	10
NMG-EGTA	0	0	115	0	1.8	10

All solutions used for this study were adjusted to pH 7.2.
NFR, normal frog Ringer; NMG, N-methyl D-glucamine; EGTA, ethylene glycol bis(β-aminoethyl ether) N, N, N′, N′-tetraacetic acid; Hepes: N-(2-hydroxyethyl) piperazine N′-(2-ethane sulfonic acid).

care was taken to prevent unstirred regions that could act as reservoirs of osmoticant.

RESULTS

Unlike previous studies in which bilateral solution changes were used to permit accurate definition of the applied osmotic stress (see Zimmerberg and Parsegian, 1986; Zimmerberg et al. 1990), the present study was initiated to study nonequilibrium effects of hyperosmolar solutions on ion channel gating. Internal versus external hyperosmolar exposure might be expected to have different effects if specific structural components involved in the gating mechanism are differentially exposed to external or internal media. To test the validity of this approach, we started by evaluating the effects of unilateral hyperosmolar exposure (~1500–2000 mOsm/kg) on the fast inactivation of wild-type *Shaker* channels, as it is already clear that inactivation occurs in these channels through a "ball-and-chain" mechanism involving protein parts that are exposed to the intracellular medium (Hoshi et al., 1990).

Effects of hyperosmolar solutions on wild-type *Shaker* B channels

Potassium currents flowing through inactivating *Shaker* B channels are shown in Fig. 1. External exposure (Fig. 1, *A–C*) to hyperosmolar solutions reduced the current magnitude without any substantial change in inactivation rate, tail current kinetics, or rate of recovery from inactivation (all parameters changed by <20%). The time course of recovery from inactivation is visualized by the envelope of peak currents during the second pulses. However, internal application of similar solutions (Fig. 1, *D–F*) produced a slowing of the time constants for fast inactivation (from 2.3 to 4.7 ms), for tail current decay (8.9 to 19.3 ms), and for the recovery from inactivation (14 to 33 ms). All osmotic effects were readily reversed by washing out the hyperosmolar medium and returning to control osmolarity.

We concluded that unilateral application of hyperosmolar solutions could be a useful tool for detailed study of the activation/deactivation mechanism, permitting potential localization of affected gating components to the internally or externally exposed surfaces of heterologously expressed *Shaker* potassium channels.

Effects of hyperosmolar solutions on channel activation

Activation/deactivation kinetics are most readily studied without the complicating effects of fast inactivation. The following work was therefore carried out using *Shaker* channel constructs in which fast inactivation has been prevented by N-terminal deletions (see Methods section). During the initial stages of this study, we attempted to assess effects of hyperosmolar solutions with total osmolarities in the range of 500-1000 mOsm/kg. However, at these osmolarities the small kinetic effects were frequently masked by random kinetic variations between successive macropatch currents. Initial studies were therefore repeated at osmolarities (between 1500 and 2000 mOsm/kg) where kinetic effects are more readily apparent.

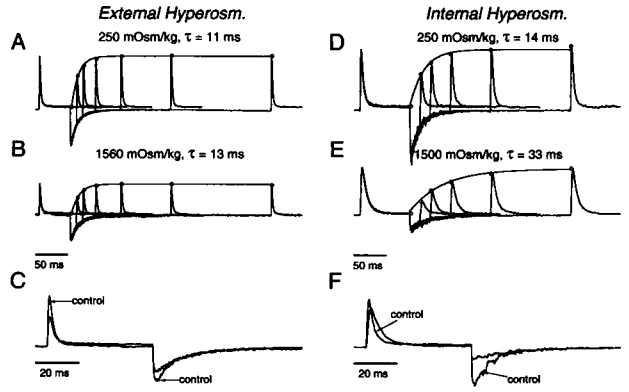

FIGURE 1 Internal application of hyperosmolar media slows inactivation and recovery from inactivation in *Shaker* B channels. Effects of external osmoticant: iso-osmolar controls (*A*) (250 mOsm/kg) are compared with traces obtained from the same outside-out patch exposed to external hyperosmolar solution (*B*) (1560 mOsm/kg). Double pulses with differing interpulse intervals were used to characterize the recovery rates. A single exponential curve has been superimposed to facilitate visualization of recovery kinetics. Single exponential fits to the recovery yielded time constants of 11 ms and 13 ms for control and hyperosmolar conditions, respectively. Individual traces from control and hyperosmotic condition are compared (*C*) by using an expanded time base. Effects of internal osmoticant: control traces (*D*) (250 mOsm/kg) are compared with traces obtained from the same inside-out patch during internal exposure to hyperosmolar solution (*E*) (1500 mOsm/kg) by using differing interpulse intervals. Time constants of recovery were 14 ms and 33 ms for control and hyperosmolar records, respectively. Control and test traces are compared (*F*) by using an expanded time base. The peak currents were suppressed in both conditions. By contrast, rates of inactivation and deactivation and the recovery from inactivation are slowed only during internal hyperosmolar exposure. Records were obtained in steps from −100 mV holding potential to +50 mV test potential; recovery potential during the interpulse interval was −140 mV in both data sets. Control solutions used here were K-Ringer//K-EGTA for both patches.

In Fig. 2, families of potassium current traces recorded from these noninactivating channels are compared before and during application of ~1600 mOsm/kg solutions to the external (Fig. 2, *A–C*) or internal (Fig. 2, *D–F*) surface of the membrane. Both external and internal hyperosmotic media suppress peak current as noted above for wild-type channels. Averaged over the entire voltage range explored, the suppression of peak conductance was asymmetrical, with 27 ± 5% suppression (mean ± SD, $n = 6$ experiments) for external application versus 41 ± 5% suppression ($n = 11$) for internal application of a 1600 mOsm/kg medium.

Noting that hyperosmolar exposure slows activation kinetics (see the scaled traces in Fig. 2, *C* and *F*), we next addressed the possibility that this slowing might result from osmotically induced changes in the voltage sensitivity of the activation mechanism. In Fig. 3, current-voltage curves that were obtained before and during both external (Fig. 3 *A*) and internal (Fig. 3 *D*) exposure to hyperosmolar solutions are

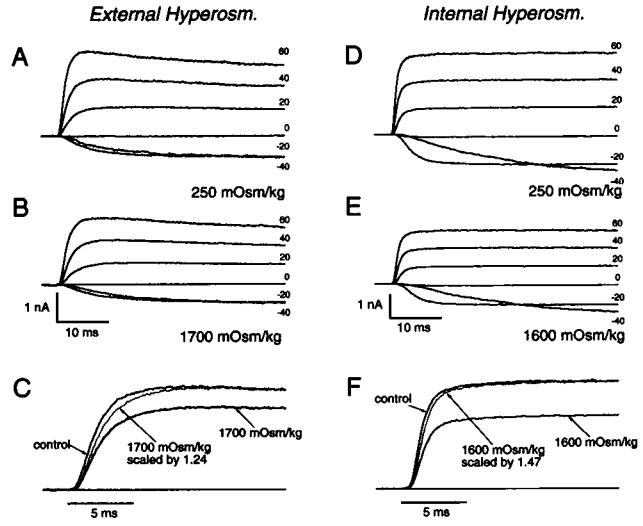

FIGURE 2 Activation is slowed by external or internal hyperosmolar media in noninactivating *Shaker* B channels. Effects of external osmoticant: current families are compared from the same outside-out patch before (*A*) (250 mOsm/kg) and during external exposure to a hyperosmolar solution (*B*) (1700 mOsm/kg). Control and test kinetics at +40 mV are compared (*C*) before and after scaling the test hyperosmolar trace (1.24-fold) to match control peak current magnitude. Effects of internal osmoticant: current families are compared from the same inside-out patch before (*D*) (250 mOsm/kg) and during internal exposure to hyperosmolar solution (*E*) (1600 mOsm/kg). Control and test kinetics at +40 mV are compared (*F*) before and after scaling (1.47-fold) to control current magnitude. Holding potential was −80 mV for both patches. Current families were obtained at 20 mV increments between −40 mV and +60 mV. Control solutions were K-Ringer//K-EGTA for both patches, giving a reversal potential of 0 mV.

shown; full recovery was obtained in both cases after washout of the experimental solutions (not shown). In both conditions, the suppression of conductance seems constant across voltage, as may be demonstrated from the voltage independence of the peak current ratios (I_{osm}/I_{contr}, see Fig. 3, *B* and *E*). Although this plot has the advantage that it is derived directly from raw data, substantial errors can occur where peak currents are small because the ratio plot is affected by the noise in both control and hyperosmolar traces. Conductance-voltage plots (not shown) from both data sets also indicate no differences from control voltage sensitivity, but the results were derived by assuming a constant single-channel conductance, which is unaffected by voltage-dependent cation block. Errors that might arise from this assumption can be minimized by measuring peak tail currents at constant return potential. Normalized peak tail currents (see Fig. 3, *C* and *F*) should directly reflect the fraction of channels open at the end of the depolarizing test pulse, and nonlinear effects of solution osmolarity on channel conductance are avoided at constant return potential. Comparison of Fig. 3, *C* and *F*, again shows that activation voltage sensitivity is not altered by hyperosmolar exposure within the range of osmolarities investigated here.

Because we find no changes in activation voltage sensitivity, osmotically induced suppression of peak current presumably arises from either changes in single-channel conductance or from changes in the probability of channel opening or from some combination of both these mechanisms. Single-channel recordings show reduction in current amplitudes during both external (Fig. 4, *A* and *B*) and internal (Fig. 4, *C* and *D*) exposure to hyperosmolar solutions. In solutions with symmetrical $[K^+]$ at +50 mV, internal exposure to 1950 mOsm/kg medium reduces the conductance by ~50%, whereas external exposure reduces the conductance by only ~25%. These values lie within the observed range of variation for suppression of peak macroscopic current by solutions of this osmolarity (see Fig. 4 *E*). This finding suggests that suppression of macroscopic currents can be largely or entirely explained by the observed changes in single-channel conductance rather than by changes in channel opening probability. Consistent with this interpretation, we note no changes in the flicker frequency (compare Fig. 4, *A–D*) during exposure to hyperosmolar solutions.

Activation kinetics also show differential effects of external versus internal application of the osmoticant (see Fig. 5). The half-activation time is increased during both internal and external hyperosmolar exposure, although the form of this slowing seems different in the two conditions. With external osmoticant (Fig. 5, *A* and *B*), the major part of the rising phase seems slowed without noticeable change in the initial sigmoid delay. By contrast, internal osmoticant (Fig. 5, *C* and *D*) seems to selectively increase the initial delay such that the major part of the rising phase seems to be parallel with the control current.

Simple quantitative description of the rising phase of potassium currents in these noninactivating channels can be achieved by fitting to the sum of three exponential components. We find that the fastest time constant (τ_1) is approximately equivalent to the delay time between the start of the voltage step and the initiation of detectable potassium current; the next time constant (τ_2) reflects the initial upswing of the potassium currents, whereas the slower component (τ_3) dominates the greater part of the rising phase. No significant improvement in the quality of fit was obtained when additional components were included (see Discussion section).

In Fig. 6 time constants obtained using three exponential fits to the rising phase of potassium current are compared for external (Fig. 6, *A–C*) versus internal (Fig. 6, *D–F*) hyperosmolar exposure. To simplify visual comparison of the results, the ratios of the osmotic/control data points are shown for each test potential in Fig. 7. In these ratio plots, a mean value of 1.0 indicates no kinetic effect, whereas a value >1.0 indicates an osmotic slowing of that parameter. The major effects seen in Fig. 7 are slowing of τ_3 by external osmoticant (approximately twofold), in contrast to a slowing of the initial delay (τ_1) and τ_2 by internal osmoticant (~1.5-fold) together with a smaller (~1.2-fold) slowing of τ_3. These findings were confirmed in a series of five experiments for each condition (see Table 2, which reports the means of the ratios from each experiment).

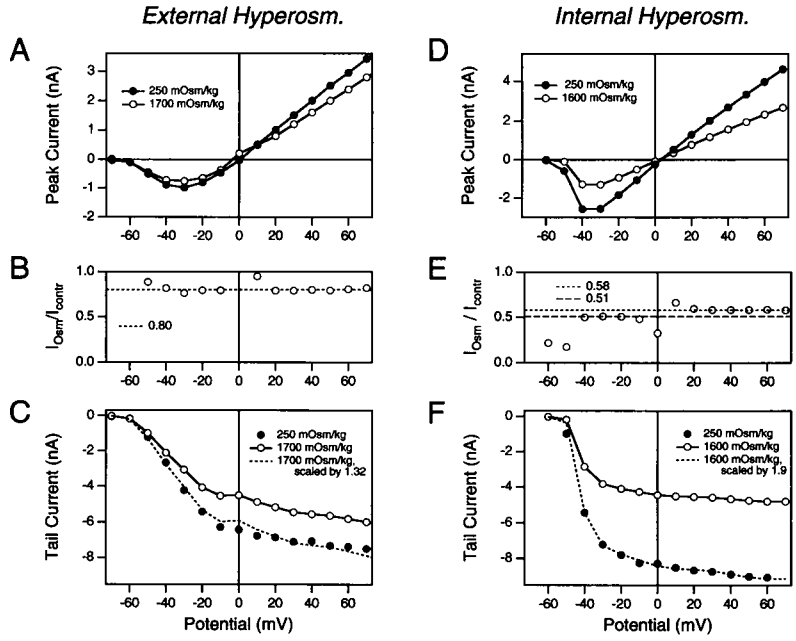

FIGURE 3 Hyperosmolar solutions suppress peak current magnitude without affecting voltage sensitivity of channel activation in noninactivating *Shaker* B channels. The current-voltage relationships for control conditions and external (*A*) (1700 mOsm/kg) or internal hyperosmolar exposure (*D*) (1600 mOsm/kg), show an osmotic suppression of peak current at all voltages. Plotting the ratios of I_{osm}/I_{contr} for each test potential shows that suppression is not voltage sensitive for either external (*B*) or internal exposure (*E*). These ratio plots also demonstrate smaller current suppression in external osmoticant (20% suppression) (*B*) compared with effects of internal osmoticant (40–50% suppression) (*E*). Peak tail currents obtained at −100 mV after each test potential during control and unilateral hyperosmolar exposure (*C* and *F*) provide an alternative approach for assessing activation voltage sensitivity. During both external (*C*) and internal (*F*) exposure scaling, the currents obtained during hyperosmolar exposure (- - - -) demonstrates no change in the voltage sensitivity of prior test pulse activation. All data were obtained by analysis of records from the same patches as shown in Fig. 2.

The amplitudes a_1, a_2, and a_3, corresponding to τ_1, τ_2, and τ_3, respectively, are complexly affected both by changes in peak current magnitude (attributable to changes in driving force at different test potentials and to hyperosmolar suppression) and by the osmotically induced kinetic changes. For outward currents, a_1 and a_3 had negative sign, with a_2 being positive. All amplitudes were smaller than 200% of the peak current. In the data of Fig. 6, the averaged ratios for a_{osm}/a_{contr} were 0.40 ± 0.13 for a_1, 0.35 ± 0.14 for a_2, and 0.46 ± 0.15 for a_3, for external hyperosmolar exposure. Corresponding ratios for internal exposure were 0.6 ± 0.25, 0.51 ± 0.19, and 0.52 ± 0.17.

In marked contrast to the differential effects of hyperosmotic media on activation rates, Fig. 8 shows that tail currents seem only minimally affected by hyperosmolar exposure (after scaling to adjust for the suppression of peak current). It should be pointed out that these tail current traces were recorded from patches that clearly demonstrated differential effects on activation kinetics equivalent to those shown in Fig. 7. The mean tail current ratio (τ_{osm}/τ_{contr}) for five experiments involving external hyperosmolar exposure was 1.03 ± 0.07, and it was 1.06 ± 0.25 for eight experiments with internal osmoticant. Because these results were all obtained with appropriate washout controls, the small

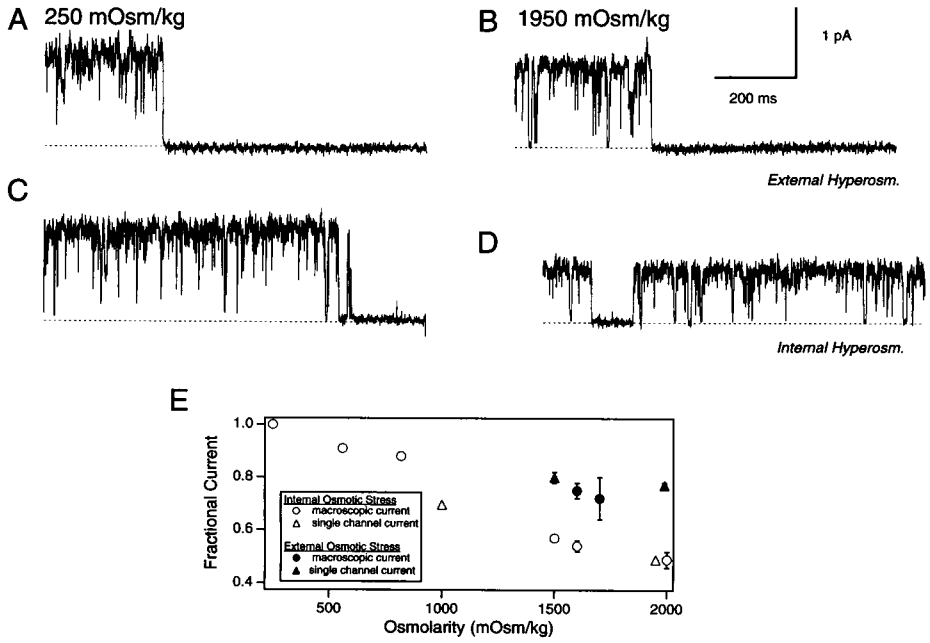

FIGURE 4 Single-channel currents and macroscopic currents show equivalent suppression by hyperosmolar solutions in noninactivating *Shaker* B channels. Single-channel currents: control records (*A* and *C*) are compared with records obtained during osmotic exposure (1950 mOsm/kg) (*B* and *D*). Greater suppression (~42%) is seen with internal osmoticant (*D*) than with external osmoticant (~11%) (*B*). Control solutions: NFR/K-EGTA for both patches. Pulses to +50 mV and filtered at 400 Hz. (*E*) Hyperosmolar solutions suppress single-channel currents (*triangles*) and macroscopic currents (*circles*) to similar extents. External exposure is indicated by filled symbols and internal exposure by open symbols. These data were obtained at +50 mV test potential with the control solutions K-Ringer//K-EGTA.

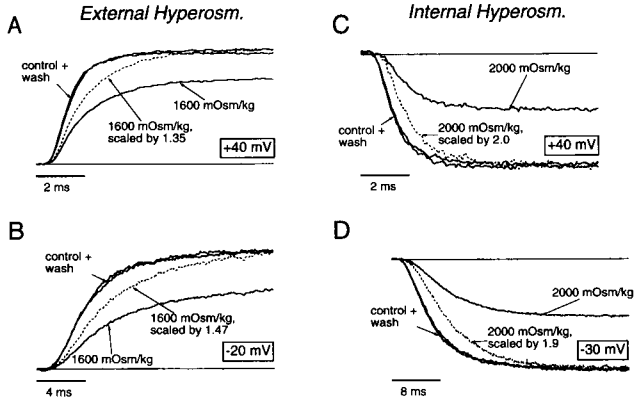

FIGURE 5 External (*A* and *B*) and internal (*C* and *D*) hyperosmotic exposure has different effects on channel activation in noninactivating *Shaker* B channels. External osmoticant: at both positive (*A*) and negative (*B*) test potentials, comparison of control and hyperosmolar (1600 mOsm/kg) traces shows a slowing involving the later part of the rising phase of potassium current. No change is apparent in the initial delay before channel activation. Compare control traces with the normalized traces (*dashed lines*) recorded during hyperosmolar exposure. Internal osmoticant: at both positive (*C*) and negative (*D*) test potentials, comparison of control and hyperosmolar (2000 mOsm/kg) traces shows that slowing of activation arises primarily from extension of the initial delay. Compare control traces with the normalized hyperosmolar traces (*dashed lines*). Holding potential was −80 mV in both experiments. For a better comparison of the effects on channel kinetics, solutions were chosen such that potassium currents flowed in both cases toward the compartments where the hyperosmolar solution was applied. Control solutions were therefore NFR//K-EGTA (*A* and *B*) and K-Ringer//NMG-EGTA (*C* and *D*).

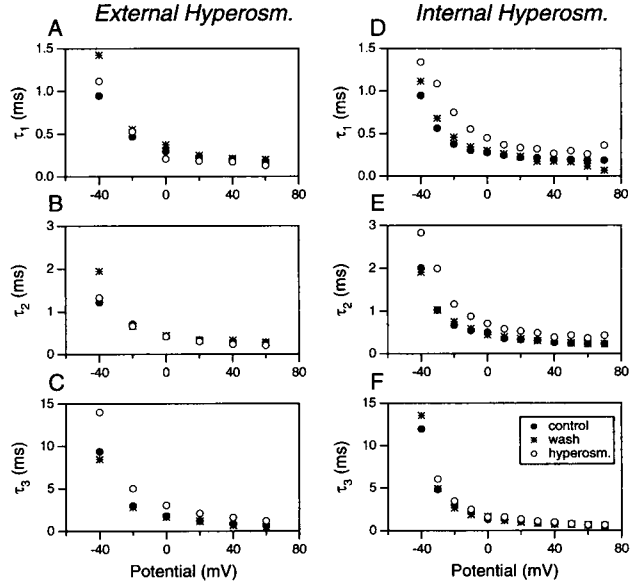

FIGURE 6 Plots of activation time constants against test potential suggest consistent differences between effects of external and internal hyperosmolar exposure. Time constants were obtained from the same two patches used for Fig. 5 by three-component exponential fitting to the activation phase of potassium currents (see Methods section); amplitudes (not shown) reflect suppression of macroscopic currents by hyperosmolar solutions (see text). External osmoticant: control data (●) and recovery data (*) are compared with data during hyperosmolar exposure (○). Note the absence of significant hyperosmolar effects in the two fastest time constants (*A* and *B*) but the clear slowing of the slowest time constant (*C*) by hyperosmolar exposure. Internal osmoticant: by contrast, internal hyperosmolar solutions slow the two fastest time constants (*D* and *E*) with little effect on the slowest time constant (*F*).

changes in tail kinetics visible in Fig. 8 may indicate minor effects beyond the resolution of the present study. Furthermore, tail current rates are quite labile even under control conditions (Sigg et al., 1994). It is apparent, however, that *Shaker* channels deactivate by a pathway that is relatively insensitive to solvent effects.

We further explored the relationship between osmotically sensitive and osmotically insensitive processes within the activation and deactivation mechanisms by using double pulse protocols. Such protocols with variable interpulse intervals were used by Alicata et al. (1990) and by Rayner et al. (1992) to show that sodium channels, which close by solvent-insensitive steps, can also reopen (secondary activation) in a solvent-insensitive manner if the interpulse interval is very brief. With longer interpulse intervals, the original solvent sensitivity of primary activation becomes reestablished. Similar effects for *Shaker* channels are shown in Fig. 9 for both external (Fig. 9, *A–C*) and internal hyperosmolar exposure (Fig. 9, *D–F*). Note that this protocol required negative interpulse potentials (−140 mV) so that the tail currents would be fast enough to minimize distortion of second pulse activation by current flowing through nondeactivated channels.

In Fig. 9, both *A* and *B*, the first depolarizing pulse demonstrates a slowing of the major rising phase kinetics (cf. Fig. 5, *A* and *B*) induced by external hyperosmolar exposure. In Fig. 9 *A*, where the interpulse interval is short (1 ms), there is no equivalent slowing of secondary activation by the hyperosmotic medium. In Fig. 9 *B*, however, the return of osmotically induced slowing was restored because the interpulse interval was increased (here shown after 32 ms). Fig. 9, *D* and *E*, show equivalent data for internal application of the hyperosmolar medium. In both traces the first depolarizing pulse shows the apparently parallel shift of the activating current phase (cf. Fig. 5, *C* and *D*). This osmotically induced slowing of activation is lost after a short interpulse interval (1 ms, Fig. 9 *D*), but returns when the interpulse interval is increased (here 32 ms, Fig. 9 *E*). The recovery of the osmotically sensitive component was estimated by plotting the differences of the current integrals during the second pulse, normalized to the end of the second test pulse, as a function of the interpulse interval (Figs. 9, *C* and *F*). Apart from the difference in the initial data points (due to incomplete channel closure during the shortest interpulse intervals; see Fig. 9 *D*), we detected no significant difference in recovery time course between external and internal hyperosmolar exposure. This result is consistent with the lack of differential effects on tail current kinetics shown in Fig. 8. Therefore, *Shaker* channels, like sodium channels, apparently close during the early steps of channel deactivation by a reversible but solvent-insensitive gating process.

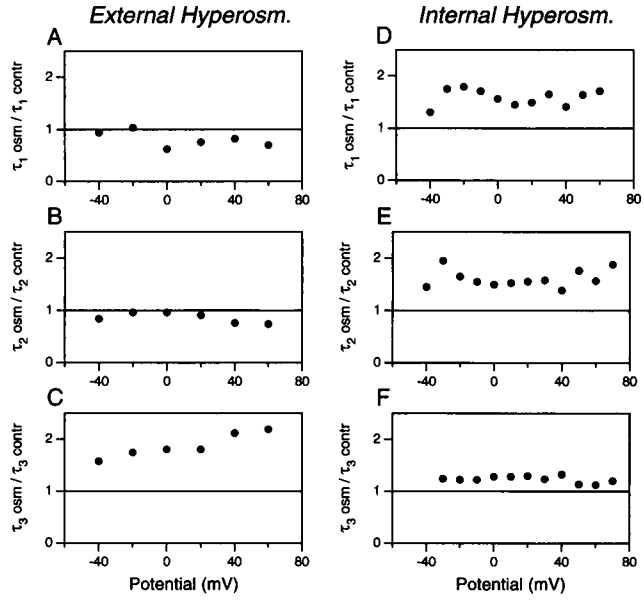

FIGURE 7 The changes in time constants shown in Fig. 6 are more readily visualized when the same data are presented as the ratio: τ_{osm}/τ_{contr}. The "τ_{contr}" values used for these ratios were calculated as the means of the time constants obtained before hyperosmolar exposure and after washout of the hyperosmolar solution. External osmoticant: the slowest time constant (*C*) is increased, whereas the two faster time constants (*A* and *B*) remain relatively unaffected. See Table 2 for mean values from five patches. Internal osmoticant: all three time constants (*D*, *E*, and *F*) are increased. Mean data from five patches (see Table 2) confirm that slowing is greatest for the fastest time constant and least for the slowest time constant.

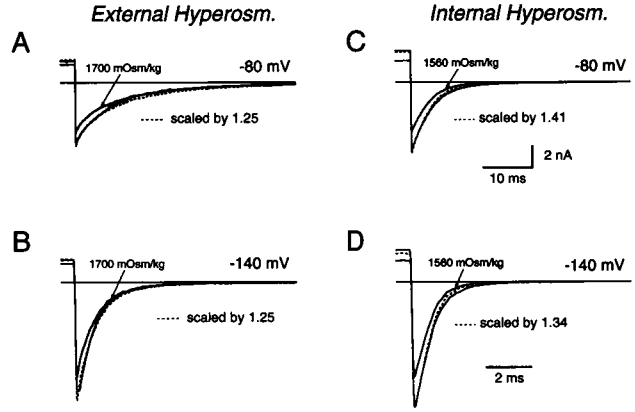

FIGURE 8 Tail current kinetics are unaffected by either external (*A* and *B*) or internal (*C* and *D*) hyperosmolar solutions in noninactivating *Shaker* B channels (cf. Fig. 1). External osmoticant: tail currents obtained before and during hyperosmolar exposure (1700 mOsm/kg) are compared at −80 mV (*A*) and −140 mV (*B*). Normalization of hyperosmolar tail to control peak (*dashed line*) demonstrates no marked kinetic changes at either return potential. Internal osmoticant: tail currents during internal hyperosmolar exposure (1560 mOsm/kg) are compared with controls at the same two return potentials (*C* and *D*). Again, the normalized trace (*dashed line*) shows no marked kinetic change. Note the different time bases used at −80 and −140 mV. Control solutions were K-Ringer//K-EGTA for both patches.

DISCUSSION

The principal results of the present study are as follows.

1) In wild-type *Shaker* channels, the time course of both inactivation and recovery from inactivation (Fig. 1) are slowed only when the hyperosmolar medium is applied to the internal surface of the membrane.

2) In noninactivating *Shaker* channels, peak macroscopic current is differentially suppressed by internal and external hyperosmolar exposure (Fig. 2). Reduction in peak current is greater for internal than for external exposure, but current suppression occurs without a detectable shift in the voltage sensitivity of channel activation (Fig. 3). Suppression of macroscopic peak currents is associated with a quantitatively equivalent suppression of single-channel conductance (Fig. 4).

3) Internal exposure to hyperosmolar media slows early steps in the activation of macroscopic current. By contrast, external exposure slows the later stages of activation (Figs. 5, 6, and 7; also Table 2).

4) Neither the tail current rates (Fig. 8) nor the rates of secondary activation (after brief interpulse intervals; see Fig. 9, *A* and *D*) are affected by hyperosmolar media.

TABLE 2 Effects of hyperosmolar solutions on activation kinetics

Patch	τ_1 Ratio	τ_2 Ratio	τ_3 Ratio
External osmoticant			
k29011cE2–1	0.88	1.09	1.55
k29013cE3–2	0.81	0.86	1.87
k29014cE2–1	0.77	0.81	3.35
k29014cE3–2	0.72	0.76	1.31
k29014cE4–3	1.20	1.09	1.89
Mean (±SD)	0.88 ± 0.19	0.92 ± 0.16	1.99 ± 0.80
Internal osmoticant			
k29001cE3–3	1.31	1.17	1.04
k29004cE4–1	1.39	1.63	1.23
k29006cE5–4	1.39	1.20	1.08
k29007cE5–4	1.69	1.61	1.23
k29008cE1–1	1.55	1.32	1.36
Mean (±SD)	1.47 ± 0.15	1.39 ± 0.22	1.19 ± 0.13

Each column shows the ratio of the respective time constant during hyperosmotic exposure and control situations. The control values were obtained by taking the average of the time constants before application of hyperosmotic solutions and after washout. Values for each patch represent the mean ratios obtained by analysis of all data traces between −20 and +80 mV (as shown in Fig. 7, these ratios are not noticeably affected by test potential).

Effects on inactivation

Asymmetric effects on channel function after application of toxins (e.g., tetrodotoxin; Narahashi et al., 1966) and proteolytic enzymes (e.g., pronase; Armstrong et al., 1973) are well documented and widely accepted as indicators of the relative accessibilities of discrete components of the gating mechanism from different sides of the membrane. The major ambiguity with this approach occurs when the agent is either permeant through ion channels or sufficiently membrane-soluble to reach its active site by other pathways (e.g., nonquarternary local anesthetics; Hille, 1977). In the

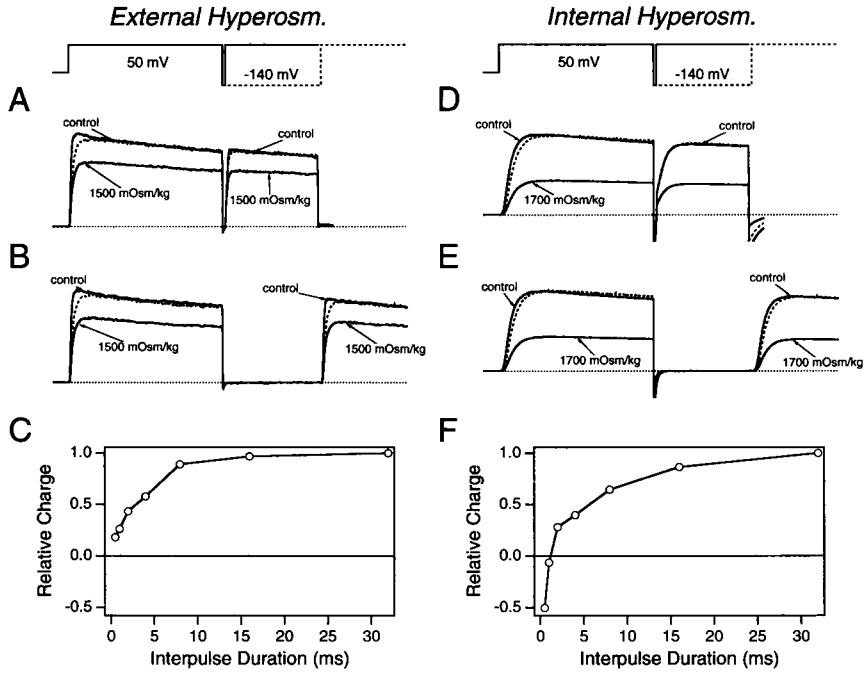

FIGURE 9 Double pulse experiments (*see pulse pattern inserts*) demonstrate the lack of osmotic sensitivity during reactivation after brief interpulse intervals for noninactivating *Shaker* B channels. Activation kinetics show return of osmotic sensitivity as the interpulse interval is increased. Return of osmotic sensitivity shows a similar time course during both external and internal hyperosmolar exposure. External osmoticant: external hyperosmolar exposure (1500 mOsm/kg) fails to slow reactivation kinetics when interpulse interval is ~1 ms (*A*). Osmotic sensitivity has returned (*B*) after a 32-ms interpulse interval at −140 mV. Relative charge movements as a function of the interpulse interval (*C*) indicate the kinetics of returning osmotic sensitivity (see below). Internal osmoticant: internal hyperosmolar exposure (1700 mOsm/kg) does not slow reactivation kinetics when interpulse interval is ~1 ms (*D*). Osmotic sensitivity has returned (*E*) after a 32-ms interpulse interval at −140 mV. Relative charge movement (*F*) indicates recovery kinetics similar to external hyperosmolar exposure. The negative points at the shortest recovery intervals result from the larger initial current step in the hyperosmolar trace, which was caused here by incomplete channel deactivation during the preceding brief interpulse interval. This would be expected if the osmoticant caused a small slowing of the deactivation kinetics. Relative charge movements (*C* and *F*) were obtained by the following procedure: traces were first normalized to equal current magnitude at the end of the second pulse; charge difference was then measured by subtraction of control and hyperosmolar traces during the second pulse; and all values were then normalized against the "steady-state" level (here obtained after 32-ms recovery intervals). Control solutions in both cases were NFR//K-EGTA.

present case, although the osmoticant is impermeant, water might cross the membrane in sufficient quantity to modify the localized effects of hyperosmolar solutions by solute dilution (see Methods section). For example, where an inside-out patch is exposed to a hyperosmolar bath, bulk movement of water inward through the channels might fully or partially wash out osmoticant molecules from the internal channel mouth. Although such water movements may occur (and may be increased or decreased by potassium current direction), water flow through the channels is not sufficient to prevent internal hyperosmolar media from affecting inactivation rates, as documented in Fig. 1.

Shaker channel inactivation (onset and recovery) is slowed by internal exposure to hyperosmotic media, paralleling a similar observation made for fast inactivation in sodium channels (Rayner et al., 1993). Furthermore, as shown in Fig. 1, *D–F*, this slowing of inactivation occurs without change in the steady-state current. These findings suggest a specific effect of the hyperosmolar medium on an energy barrier within the inactivation mechanism rather than either a shift in voltage sensitivity or a change in binding site affinity, i.e., the change in energy of the inactivated state. Both of these latter mechanisms would predict that where onset of inactivation is slowed, recovery should be speeded by hyperosmotic media.

In Fig. 1, it was noted that internal (but not external) exposure to hyperosmolar media has marked effects on the kinetics of tail currents in wild-type *Shaker* B channels. Because no equivalent sensitivity to hyperosmotic media appears in tail currents of inactivation-removed mutant channels (Fig. 8), the slow tails in the wild-type channels presumably result from osmotically induced slowing of the recovery from inactivation (Fig. 1), as would be expected inasmuch as A-type potassium channels are known to open transiently during recovery from inactivation (Ruppersberg et al., 1991).

The suppression of macroscopic currents

In unilaterally exposed *Shaker* channels, osmotically induced suppression of peak macroscopic current seems to be associated with suppression of single-channel conductance rather than with any detectable changes in equilibrium gat-

ing properties (Fig. 4). Additionally, Heinemann (1995) has reported the results of nonstationary noise analysis of outward potassium currents flowing through *Shaker* BD6–46 channels, before and after internal exposure to a 2000 mOsm/kg sucrose medium. The ensemble variance from macropatch currents obtained during steps to +80 mV were plotted as a function of mean current for both control and hyperosmolar conditions. Fits to these curves yielded estimates both for single-channel currents (1.78 pA for the control and 1.14 pA during internal hyperosmolar exposure) and for maximal channel open probabilities (0.78 in both cases). This 40% suppression of single-channel conductance was exactly matched by a similar suppression of macroscopic current.

The observed suppression of macroscopic current in *Shaker* channels during unilateral internal hyperosmotic exposure seems similar in magnitude to the effects of bilateral osmotic stress in squid delayed-rectifier channels. Table 2 of Zimmerberg et al. (1990) presents data showing that adding 1000 mOsm/kg of sucrose to bilateral solutions already containing 1000 mOsm/kg sucrose gave an additional ~50% reduction in macroscopic current. For comparison, Shaker channel data (see Fig. 4) suggests that increasing internal sucrose concentration (from 1000 to 2000 mOsm/kg) should cause an additional ~40% current suppression.

Suppression of single-channel conductance might result from reduced conductivity of hyperosmolar solutions or from changes in channel permeability or both. At the macroscopic level, Zimmerberg et al. (1990) noted that different osmoticants produced differing changes in solution conductivity and undertook a careful comparison of the relative effects of osmolarity versus conductivity in their solutions. For internal hyperosmolar media, they found that macroscopic current suppression was determined solely by osmolarity and was unaffected by changes in conductivity. By contrast, both osmolarity and conductivity altered the suppression of current produced by external hyperosmolar media (in squid axon delayed-rectifier channels). They concluded that solution conductivity changes are normally inconsequential in comparison with the major current-limiting resistance provided by ion channel permeation. However, in axonal preparations, in which external osmoticants may cause narrowing of current pathways between Schwann cells, significant changes in external series resistance have been demonstrated (Stimers et al., 1987; Alicata et al., 1989). Such changes in series resistance could magnify the effect of conductivity changes in the external medium for axonal preparations.

In excised patches, we note that single-channel amplitudes are differentially affected by external and internal osmotic exposure (see Fig. 4). These disparities could result from effects of conductivity acting within the differing geometries of the internal and external channel mouths. Anderson (1983) has demonstrated that both sucrose and urea can limit the single-channel conductance of gramicidin A channels by reducing diffusive ion movements through the aqueous convergence regions that must be traversed by ions approaching the channel entrance. Alternatively, the observed suppression of single-channel conductance could result, wholly or partially, from changes in ion transport parameters within the pore region of the channel.

Regardless of the detailed mechanism by which single-channel current is suppressed, the quantitative equivalence of single-channel and macroscopic current suppressions in *Shaker* channels shown here (see Fig. 4), together with the lack of effect on channel open probabilities (Heinemann, 1995), clarifies that suppression of macroscopic current involves no significant changes in the channel opening probability under conditions of unilateral hyperosmolar exposure. Nevertheless, in view of the osmotic gradients that may be predicted to occur within the permeation pathway of unilaterally exposed ion channels, these findings do not provide sufficient evidence from which to infer that the macroscopic current suppression produced by well defined, bilateral osmotic stress can be similarly explained solely by changes in single-channel conductance.

Effects of unilateral hyperosmolar exposure on activation/deactivation kinetics

Excluding effects specifically related to fast inactivation, all voltage-gated channels so far investigated show similar kinetic responses to hyperosmolar exposure: activation is slowed, with little or no effect on tail-current deactivation rates. An equivalent pattern of kinetic changes has been noted previously for effects of D_2O on sodium channels (Schauf and Bullock, 1982; Alicata et al., 1990), as well as for osmotic effects on both delayed-rectifier potassium channels (Zimmerberg et al., 1990) and sodium channels (Rayner et al., 1992).

By using unilateral exposure to hyperosmolar media, we have shown additional selective effects on kinetic components of the activation/deactivation mechanism. As seen in Figs. 6 and 7, external exposure slows the late rising phase of activation, whereas internal exposure produces an increased delay in the onset of potassium currents and a "parallel" shift in the major part of the rising phase, similar to the Cole-Moore shifts (Cole and Moore, 1960) found at hyperpolarized resting potentials. This finding suggests a structural separation between the mechanisms responsible for the initial activation delay and the later rising phase of ionic current. Similarly, Conti et al. (1982a,b), who applied high hydrostatic pressures to squid axons so as to evaluate volume changes during channel gating in both sodium and delayed-rectifier channels, found that the initial activation delay in both channel types was less pressure sensitive than the later part of the rising phase. We note that the greater pressure sensitivity of the late activation kinetics seems consistent with a mechanistic separation between the early and late components of channel activation, suggesting a greater volume change (and hence a larger conformational change) associated with the final steps of the activation mechanism.

In the present study, osmotically induced changes in activation rates occurred without detectable changes in activation voltage sensitivity (see Fig. 3). Furthermore, the data showing the effects of hyperosmolar solutions on single-channel conductance and channel open probability (Fig. 4 and Heinemann, 1995) must argue against any changes in equilibrium gating for unilaterally exposed channels. Presumably, therefore, the kinetic effects of unilateral exposure to hyperosmolar sucrose are mediated by changes in energy barrier heights for either early steps in channel activation (during internal exposure) or late steps (during external exposure).

We chose to quantify changes in activation kinetics, using the simplest method that could provide accurate descriptions of the sigmoid ionic currents seen in noninactivating *Shaker* channels. Our currents were well fitted by the sum of three exponential components. As noted in the Results section, the first time constant (τ_1) corresponds approximately to the delay time before the start of visible potassium current; the next time constant (τ_2) reflects the fast initial rise time of ionic current; and finally, τ_3 characterizes the major part of the rising phase of potassium current. The accuracy of our fits was not improved by including additional exponential components. Applying this analysis to currents obtained at test potentials across a range of ~100 mV (see Figs. 6 and 7) confirms that external hyperosmolar exposure mainly slows the major activation kinetic (τ_3). By contrast, internal osmotic exposure increases the initial delay (τ_1) and slows the early sigmoid onset of activation (τ_2) with a consistently smaller effect on τ_3. When ratios of the parameter values under test/control conditions were used to remove the kinetic variability between experiments, these findings were confirmed in a series of five experiments for each condition (see Table 2).

The accurate fits obtained by using this simple descriptive analysis may seem surprising in view of the theoretical complexity of recent multistate potassium channel models (McCormack et al., 1994; Zagotta et al., 1994). However, the kinetic complexity of such models may be reduced where the predicted eigenvalues reflect some smaller number of "functional mechanisms," within which the dominant transitions show closely similar rates and similar susceptibilities to (for example) internal or external hyperosmolar media. Thus we find that simulations of potassium current activation obtained by using a cyclic 10-state model (see Fig. 10) are, like our experimental data, well described by the sum of three exponential terms.

Additionally, our findings (see Figs. 8 and 9) clarify that the rates of both deactivation and deactivation reversal (i.e., reactivation after brief interpulse intervals) are relatively insensitive to hyperosmolar effects from either side of the membrane. Thus the initial step in channel deactivation

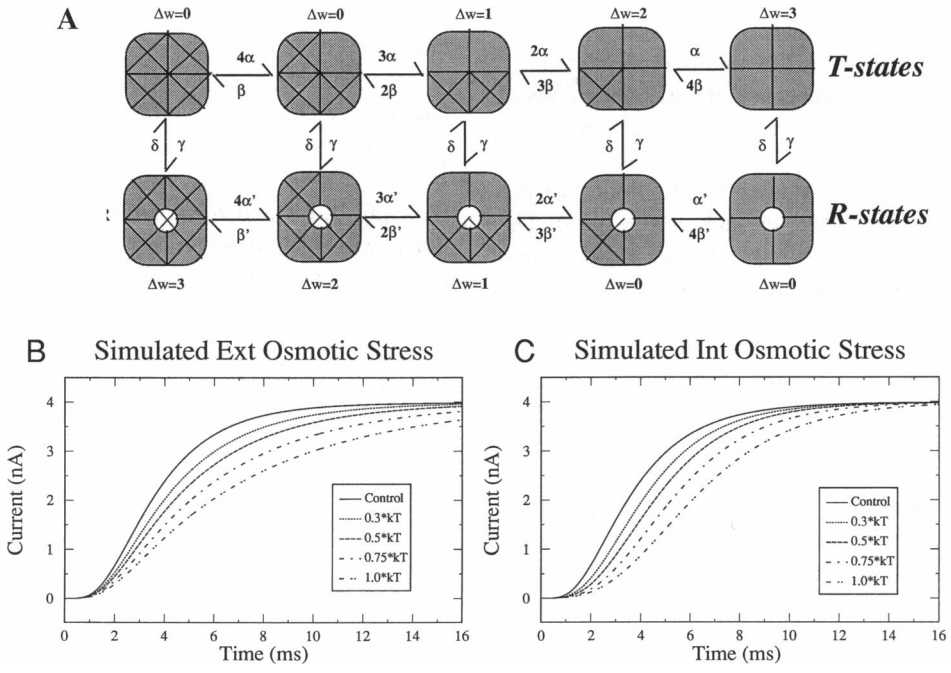

FIGURE 10 Simulated potassium currents obtained by using a cyclic *T-R* model (*A*). Simulated effects of external (*B*) and internal (*C*) exposure to osmoticant are shown here for comparison with experimental data (see Figs. 2 and 5). Simulations were run for steps from a holding potential of −100 mV to +40 mV test potential, followed by a return step to −100 mV, presuming a reversal potential of 0 mV. Initial conditions at holding potential were obtained by prior simulations. Clamp settling time was assumed to be ~100 ms for these voltage steps, with clamp rise kinetics closely matching those seen in the experimental data. All tail currents were identical to their corresponding controls and have therefore been omitted from this figure. External osmoticant (*B*): as noted in the text, effects of external osmoticant were simulated by increasing barrier height for all *T-R* transitions. Effects of increasing these barriers by 0.3, 0.5, 0.75, and 1.0 kT units are shown here. Internal osmoticant (*C*): effects of internal osmoticant were simulated by increasing barrier height for all *T*-state transitions. Barrier increments were the same as for external osmotic exposure. See text and Table 3 for simulation methods and control simulation parameters.

must reflect a functional mechanism different from the osmotically sensitive transitions, which are rate-limiting during channel activation. This conclusion seems model-discriminatory in that it must argue against any model in which an osmotically sensitive step is proposed as the first step in channel deactivation (at the negative return potentials used in this study).

A biophysical model for effects on activation/deactivation kinetics

Zimmerberg et al. (1990) and Rayner et al. (1992) argued that hyperosmolar suppression of macroscopic current resulted from changes in the open-channel probability, concluding that the open and closed states must differ in their degree of hydration. By contrast, in unilaterally exposed *Shaker* channels in which osmotically induced changes in single-channel conductance can largely explain the suppression of macroscopic conductance, the observed changes in activation kinetics presumably arise from an osmosensitivity of the energy barriers rather than from changes in the probability for finding a channel in the open state. Apparently, it is the activation energy of the transition states that is affected, as if such transitions necessitate the movement of a charged "particle" across a space in which it is partially (or fully) exposed to the surrounding solvent. Such a particle would require hydration while in transit, and the probability of such a transition occurring in a given time would be dependent on the energy cost of this hydration step.

We have explored the hypothesis that early transitions in the activation sequence are physically, and perhaps structurally, separable from both the late activation transitions and the deactivation process, using a cyclic model for potassium channel activation (McCormack et al., 1994). The central assumptions of that model are 1) that *Shaker* channels exist in two different quarternary conformations, a *Tense* (nonopenable) conformation favored at resting potential and a *Relaxed* (potentially openable) conformation favored at depolarized potentials; 2) that each of these quarternary conformations includes as many as five thermodynamically separable states resulting from voltage-induced activation of successive channel monomers; 3) that activation of each monomer requires a charge movement equivalent to 2.3 electron charges (e_0) crossing the transmembrane field; and 4) that the coordinated transition between *Tense* (*T*) and *Relaxed* (*R*) quarternary conformations involves ~10% of the total gating charge (i.e., ~1 e_0) and is selectively blocked by 4-aminopyridine (see McCormack et al., 1994). In this model, channel activation involves *T*-state transitions followed later by the coordinated *T-R* step, whereas deactivation is initiated by *R*-state transitions, which then trigger reversal of the *T-R* conformational step. Fig. 10 *A* presents a modified version of this cyclic *T-R* model.

It should be noted that both the model of Fig. 10 *A* and the model used by McCormack et al. (1994) are substantially different from the class C models evaluated and dismissed by Zagotta et al. (1994) in which all relaxed states were presumed to be open and conducting. Unlike those class C models, the model used here predicts appropriately sigmoidal activation kinetics (see Fig. 10, *B* and *C*).

For this model to favor the *Tense* conformation when hyperpolarized and the openable *Relaxed* conformation when depolarized, some interactive coupling must occur between individual monomers. For example, if monomer activation resulted from S4-segment movements, then S4 segments in the *Tense* conformation might be arranged such that they repel each other when they reach their depolarization-favored positions; by contrast, the S4s of the *Relaxed* conformation might repel each other only in their hyperpolarization-favored positions. McCormack et al. (1994) expressed such monomer coupling in the *R* and *T-R* transitions by phenomenological constants (k and k' in their terminology). Here we have chosen to include symmetrical coupling for both *T* and *R* states, which is expressed as a change in the well energies (Δw) for affected states (see Fig. 10 *A* and Table 3).

Defining $k_{1,2}$ as the rate constant for the depolarization-favored transition between any two states within this model (i.e. α, α', or γ in Fig. 10 *A*) and $k_{2,1}$ as the reverse rate constant between these same two states, (i.e., β, β', or δ in Fig. 10 *A*), then:

$$k_{1,2} = kT/h \cdot \exp((-b_{1,2} + w_1 + \Delta w_1 + qdV)/kT) \quad (1)$$

$$k_{2,1} = kT/h \cdot \exp((-b_{1,2} + w_2 + \Delta w_2 - q(1-d)V)/kT) \quad (2)$$

where k, T, and h have their usual significance; $b_{1,2}$ is barrier height, and w_1 and w_2 are the well energies for these states; q is the effective gating charge for the transition ($2.3e_0$ for all *T* and *R* transitions and $1.0e_0$ for *T-R* transitions; see McCormack et al., 1994); d represents the position of the energy barrier along the reaction coordinate from

TABLE 3 Parameters used for simulations of experimental data (see Fig. 10)

	States	1	2	3	4	5
T states	w	8	4	0	−4	−8
	Δw	0	0	1	2	3
	Total	8	4	1	−2	−5
R states	w	6	2	−2	−6	−10
	Δw	3	2	1	0	0
	Total	9	4	−1	−6	−10

All values are given in kT units. Barrier heights (b) were uniform for each transition type: 25 kT units for both *T* state and *R* state transitions and 27 kT for the *T-R* transitions. However, these uniform barriers were added to the well energy of the hyperpolarization-favored state, such that $b_{1,2}$ in Eqs. 1 and 2 was calculated as ($b + w_1$); thus, for the transition from T_1 to T_2, $b_{1,2}$ would be 33 kT units.

Note: the model presented schematically in Fig. 10 *A* is shown in a reduced form where, for example, the T_2 state (second from the left) represents all four of those analytically separable states in which only one of the four monomers has been activated. However, our simulations were run using the full 32-state model.

the depolarization-favored energy well (here assumed to be 0.5 for all transitions); V is the applied membrane potential, and Δw describes the (negative) cooperativity between monomers as an increase in well energy for each affected state. Simulation parameters are given in Fig. 10 *A* and in Table 3.

Initial simulations using the model shown in Fig. 10 *A* demonstrated that for this model the early sigmoidal kinetics of activation depend primarily on monomer activation within the *Tense* conformation (see Fig. 10 *B*). However, the greater part of the rising phase of activation is controlled by the slower coordinated transitions between the *Tense* and *Relaxed* pathways. By contrast, on return to negative holding potentials, the initial channel-closing steps involve only rapid monomer deactivations within the *Relaxed* conformation. These properties of the cyclic *T-R* model suggested that internal hyperosmolar exposure might be simulated by increasing the barrier heights for the *T* transitions, whereas external exposure might be modeled by a selective increase in the *T-R* barriers, leaving the *R* transitions unaffected by hyperosmolar media. (Parameters used for control simulations are shown in Table 3.)

In Fig. 10, simulated current traces are shown that were obtained by utilizing these simple assumptions. Effects of external osmoticant (see Fig. 10 *B*) were modeled by assuming identical increases in all *T-R* barriers, from 27 kT units for the control curve to 27.3, 27.5, 27.75, and 28 kT units. Similarly, effects of internal osmoticant (see Fig. 10 *C*) were simulated by equivalent additions of 0.3, 0.5, 0.75, and 1.0 kT units to the control 25 kT unit *T*-state barriers. Simulated tail currents (not shown) were completely unaffected by these changes. Three exponential fits to the activation simulations shown in Fig. 10, *B* and *C*, fall within the thickness of the lines used in those figures. The time-constant changes produced by these simulated osmotic exposures (see Table 4) are similar in form to those shown in Table 2. Quantitative comparisons between Tables 2 and 4 suggest that the kinetic changes produced by ~1500 mOsm/kg solutions would be best matched by increases of about 0.6 kT units in the *T-R* barriers (for external osmotic exposure) and 0.3 kT units for the *T*-state barriers (for internal exposure).

TABLE 4 Analysis of simulated data from Fig. 10

Barrier increase (kT units)	τ_1 Ratio	τ_2 Ratio	τ_3 Ratio
External osmoticant			
0.3	0.90	1.03	1.35
0.5	0.97	0.95	1.66
0.75	0.90	0.97	2.13
1.0	0.96	0.89	2.73
Internal osmoticant			
0.3	1.43	1.39	0.94
0.5	1.69	1.66	0.94
0.75	1.83	1.87	1.10
1.0	2.40	2.24	1.18

This Table presents the results of three-component analysis of the simulated data shown in Fig. 10. Effects of barrier height increases (shown) are presented as the ratio (τ_{test}/τ_{contr}) just as for the experimental data shown in Table 2. Simulation assumptions are described in the text, simulation parameters are shown in Table 3.

Note: this model produces slightly smaller effects on τ_3, after slowing of τ_1 and τ_2 by increase in *T*-state barrier heights, than is evident in the data (see Table 2).

Despite 1) the model-dependent nature of these simulation parameters and 2) our present inability to define a quantitative osmotic stress resulting from unilateral exposure of the channel molecules, our simulations may offer at least a preliminary indication as to the magnitude of the osmotic effect. Presuming that the effects of sucrose are purely osmotic (see Methods section) and applying the logic used by Zimmerberg et al. (1990), where P_{osm} is the osmotic pressure of the medium, where ν_{osm} is a solute-inaccessible volume associated with the transition state, and where m_o is the intrinsic energy of the transition state, then the total energy (m_t) of the transition state will be:

$$\mu_t = (\mu_o + \Pi_{osm} \cdot \nu_{osm}) \quad (3)$$

Thus the change in barrier height for change from the control medium (Π_{osm1}) to the hyperosmolar medium (Π_{osm2}) should be:

$$\Delta\mu_t = \nu_{osm}(\Pi_{osm2} - \Pi_{osm1}) \quad (4)$$

Solving Eq. 4 for ν_{osm}, where $\Delta\mu_t$ is 0.6 kT, suggests a solute-inaccessible volume of 0.72 nm^3 (or ~24 water molecules) for the coordinated *T-R* transition. Similarly, for a barrier height change of 0.3 kT, 12 waters would be involved during the activation of each monomer within the *Tense* conformation. Thus these figures suggest a total solute-inaccessible volume of about 2.2 nm^3, requiring movement of ~70 water molecules. This estimate of the solute inaccessible volume is reasonably consistent with those reached in previous studies (~0.7–~1.3 nm^3), even though we here detect no apparent difference in the equilibrium hydration energies of the closed and open channel conformations. However, if the deactivation process initially involves only transitions within the *Relaxed* conformational state (which do not seem to involve solvent-charge interactions), then only the final reversal of the *T-R* transition might involve water movements during channel deactivation. This process could be weighted too little in the ionic tail currents for its osmosensitivity to be readily detectable, and no kinetic changes are visible in simulated tail currents, even for 1.0-kT increases in the *T-R* barriers. However, we found minor changes in the later components of the tail currents during external osmotic exposure (see Fig. 8, *A* and *B*) that may result from slowing of the *T-R* transitions.

The conclusions reached here have potential structural implications. First, major functional parameters (early activation, late activation, and deactivation) seem to be structurally separable in that they are differentially affected by internal versus external osmoticants. Second, the conformational changes involved in monomer activation (which transport at least $2e_0$/monomer across the voltage field) involve measurable changes in channel hydration and thus

may be associated with substantial movements of charge in, or in close proximity to, the intracellular solvent. Third, the final step(s) of channel activation similarly show detectable osmotic sensitivity; in this case however, the associated charge movements interact principally with the extracellular solvent during a larger conformational change than that involved in monomer activation. Fourth, the apparent lack of osmotic sensitivity during channel deactivation suggests that charges returning during this phase are moving within a different quarternary structure than that encountered during channel activation. Finally, despite the interactions between charge movements and solvent molecules that occur during major state transitions within the gating process, we detect no effects that would indicate substantial differences between the hydration energies of the closed and open states of the *Shaker* channel under conditions of unilateral hyperosmotic exposure.

This last finding might seem to rule against structural models that predict substantial collapse of the ion permeation pathway during entry into the closed state. However, such a conclusion would be premature. As discussed here, osmotic gradients across the membrane may result in effective washout of osmoticant from within the permeation pathway. Additionally, it is also possible that dehydration within part (or all) of the permeation path might be approximately balanced by compensatory exposure of alternative hydratable sites on the outer sides of a "collapsed," dehydrated, channel. Additional work will be required to address these possibilities.

Special thanks are extended to Dr. Walter Stühmer and Dr. Erwin Neher for their hospitality and lab space at the Max Planck Institute in Göttingen. We are grateful to Dr. Ken McCormack for generously providing the *Shaker* 29–4 cDNA. Our appreciation is also extended to Dr. Peter Ruben, Mark Henteleff, and Marilou Andres for their assistance in this project. The study was supported in part by National Institutes of Health Grants R01-NS21151 (to J. G. Starkus) and RO1-NS29204 (to P. C. Ruben), National Institutes of Health RCMI Grant RR-03061, the Max Planck Society, and the American Heart Association Hawaii Affiliate.

REFERENCES

Alicata, D. A., M. D. Rayner, and J. G. Starkus. 1989. Osmotic and pharmacological effects of formamide on capacity current, gating current, and sodium current in crayfish giant axons. *Biophys. J.* 55:347–353.

Alicata, D. A., M. D. Rayner, and J. G. Starkus. 1990. Sodium channel activation mechanisms. Insights from deuterium oxide substitution. *Biophys. J.* 57:745–758.

Anderson, O. S. 1983. Ion movement through gramicidin A channels. Studies on the diffusion-controlled association step. *Biophys. J.* 41: 147–165.

Armstrong, C. M., F. Bezanilla, and E. Rojas. 1973. Destruction of sodium conductance inactivation in squid axons perfused with pronase. *J. Gen. Physiol.* 62:375–391.

Cole, K. S., and, J. W. Moore. 1960. Potassium ion current in the squid giant axon: dynamic characteristic. *Biophys. J.* 1:1–14.

Colombo, M. F., D. C. Rau, and V. A. Parsegian. 1992. Protein solvation in allosteric regulation: a water effect on hemoglobin. *Science.* 256: 655–659.

Conti, F., R. Fioravanti, J. R. Segal, and W. Stühmer. 1982a. Pressure dependence of the sodium currents of squid giant axon. *J. Membr. Biol.* 69:23–34.

Conti, F., R. Fioravanti, J. R. Segal, and W. Stühmer. 1982b. Pressure dependence of the potassium currents of squid giant axon. *J. Membr. Biol.* 69:35–40.

Hamill, O. P., A. Marty, E. Neher, B. Sakmann, and F. J. Sigworth. 1981. Improved patch-clamp techniques for high-resolution current recording from cells and cell-free membrane patches. *Pflügers Arch.* 391:85–100.

Heinemann, S. H. 1995. Guide to data acquisition and analysis. *In* Single Channel Recording, 2nd ed. B. Sakmann and E. Neher, editors. Plenum Press, New York. 53–91.

Hille, B. 1977. Local anesthetics: hydrophilic and hydrophobic pathways for the drug-receptor reaction. *J. Gen. Physiol.* 69:497–515.

Hoshi, T., W. N. Zagotta, and R. W. Aldrich. 1990. Biophysical and molecular mechanisms of *Shaker* potassium channel inactivation [see comments]. *Science.* 250:533–538.

Iverson, L. E., and B. Rudy. 1990. The role of divergent amino and carboxyl domains on the inactivation properties of potassium channels derived from the *Shaker* gene of Drosophila. *J. Neurosci.* 10:2903–2916.

Kornblatt, J. A., and G. H. B. Hoa. 1990. A nontraditional role for water in the cytochrome *c* oxidase reaction. *Biochemistry.* 29:9370–9376

McCormack, K., W. J. Joiner, and S. H. Heinemann. 1994. A characterization of the activation structural rearrangements in voltage-dependent *Shaker* K^+ channels. *Neuron.* 12:301–315.

Methfessel, C., V. Witzemann, T. Takahashi, M. Mishina, S. Numa, and B. Sakmann. 1986. Patch clamp measurements on *Xenopus laevis* oocytes: currents through endogenous channels and implanted acetylcholine receptor and sodium channels. *Pflügers Arch.* 407:577–588.

Narahashi, T., N. C. Anderson, and J. W. Moore. 1966. Tetrodotoxin does not block excitation from inside the nerve membrane. *Science.* 153:765–767.

Parsegian, V. A., R. P. Rand, and D. C. Rau. 1986. Osmotic stress for the direct measurement of intermolecular forces. *Methods Enzymol.* 127:400–416.

Rayner, M. D., J. G. Starkus, P. C. Ruben, and D. A. Alicata. 1992. Voltage-sensitive and solvent-sensitive processes in ion channel gating. Kinetic effects of hyperosmolar media on activation and deactivation of sodium channels. *Biophys. J.* 61:96–108.

Rayner, M. D., J. G. Starkus, and P. C. Ruben. 1993. Hydration forces in ion channel gating. *Comments Mol. Cell. Biophys.* 8:155–187.

Ruppersberg, P. J., R. Frank, O. Pongs, and M. Stocker. 1991. Cloned neuronal IK(A) channels reopen during recovery from inactivation. *Nature.* 353:657–660.

Schauf, C. L., and J. O. Bullock. 1982. Solvent substitution as a probe of channel gating in Myxicola. Effects of D_2O on kinetic properties of drugs that occlude channels. *Biophys. J.* 37:441–452.

Schoppa, N., K. McCormack, M. A. Tanouye, and F. J. Sigworth. 1992. Size of gating charge in wild-type and mutant *Shaker* potassium channels. *Science.* 255:1712–1715.

Sigg, D., F. Bezanilla, and E. Stefani. 1994. Slowing of deactivation kinetics in *Shaker* B as seen in macropatch recordings of gating and ionic currents. *Biophys. J.* 66:439*a*. (Abstr.)

Starkus, J., T. Schlief, and S. H. Heinemann. 1994. Effects of high osmotic stress on *Shaker* K channels. *Biophys. J.* 66:211*a*. (Abstr.)

Starkus, J. G., T. Schlief, M. Rayner, and S. H. Heinemann. 1995. Unilateral exposure to hyperosmotic stress: effects on *Shaker* B potassium channels. *Biophys. J.* 68:31*a*. (Abstr.)

Stimers, J. R., F. Bezanilla, and R. E. Taylor. 1987. Sodium channel gating currents. Origin of the rising phase. *J. Gen. Physiol.* 89:521–540.

Stühmer, W., C. Methfessel, B. Sakmann, M. Noda, and S. Numa. 1987. Patch clamp characterization of sodium channels expressed from rat brain cDNA. *Eur. Biophys. J.* 14:131–138.

Zagotta, W. N., T. Hoshi, and R. W. Aldrich. 1994. *Shaker* potassium channel gating III: evaluation of kinetic models for activation. *J. Gen. Physiol.* 103: 321–362.

Zimmerberg, J., and V. A. Parsegian. 1986. Polymer inaccessible volume changes during opening and closing of a voltage-dependent ionic channel. *Nature.* 323:36–39.

Zimmerberg, J., F. Bezanilla, and V. A. Parsegian. 1990. Solute inaccessible aqueous volume changes during opening of potassium channel of the squid giant axon. *Biophys. J.* 57:1049–1064.